

RESEARCH ARTICLE

Effects of low-dose energy spectrum scanning combined with adaptive statistical iterative reconstruction on the quality of imaging in Budd-Chiari syndrome

Lei Su¹ , Liyang Chang¹ , Qiang Sun², Lili Hu¹, Yan Wu¹, Jianbo Gao¹ *

1 Department of Radiology, First Affiliated Hospital of Zhengzhou University, Zhengzhou, Henan Province, China, **2** Department of Stomatology, First Affiliated Hospital of Zhengzhou University, Zhengzhou, Henan Province, China

 These authors contributed equally to this work.

* 878574853@qq.com



 OPEN ACCESS

Citation: Su L, Chang L, Sun Q, Hu L, Wu Y, Gao J (2018) Effects of low-dose energy spectrum scanning combined with adaptive statistical iterative reconstruction on the quality of imaging in Budd-Chiari syndrome. PLoS ONE 13(10): e0204797. <https://doi.org/10.1371/journal.pone.0204797>

Editor: Nick Todd, Brigham and Women's Faulkner Hospital, UNITED STATES

Received: April 2, 2017

Accepted: September 14, 2018

Published: October 18, 2018

Copyright: © 2018 Su et al. This is an open access article distributed under the terms of the [Creative Commons Attribution License](https://creativecommons.org/licenses/by/4.0/), which permits unrestricted use, distribution, and reproduction in any medium, provided the original author and source are credited.

Data Availability Statement: All relevant data are within the paper and its Supporting Information files.

Funding: This work was supported by grants of the National Natural Science Foundation of China (NSFC 81402231, 31400839), the basic and frontier technology research projects by Science and Technology Department of Henan province (142300410315) and the funding from Youth Foundation of The First Affiliated Hospital of

Abstract

Objective

To assess the quality and diagnostic accuracy of monochromatic images combined with adaptive statistical iterative reconstruction (ASIR) performed via spectral computed tomography (CT) in patients with Budd-Chiari syndrome (BCS).

Methods

Sixty-two patients with BCS underwent spectral CT with upper abdominal two-phase contrast-enhanced scanning to generate a 60keV monochromatic energy level combined with ASIR (ranging from 0% -100%) during the portal venous phase (PVP) and the hepatic venous phase (HVP). One-way ANOVA was used to compare vessel-to-liver contrast-to-noise ratio (CNR) for the portal vein (PV), hepatic vein (HV), and inferior vena cava (IVC). Subjective evaluations of the images in the three groups were conducted by image quality assessors and compared via Kruskal-Wallis H test.

Results

The CNR values of the PV trunk, HV, IVC, liver parenchyma and pancreas were within ASIR (ranging from 0% - 100%) weight, and the difference were statistically significant ($p < 0.05$). The highest overall image score was distributed at 50% ASIR weight value. Higher CNR values of HV, hepatic parenchyma and pancreas were obtained in the IVC type than in mixed and HV types (respective p values = 0.035, 0.019 and 0.042). Higher CNR values of the IVC were obtained in the HV type than in mixed and IVC types ($p = 0.032$). The CNR value of the IVC in the mixed type was less than that of the HV type ($p = 0.028$). The CNR values of the HV and liver parenchyma in mixed type were lower than those of the IVC type ($p = 0.016$ and 0.038, respectively). The CNR value of pancreas in IVC type was higher than that of the HV type ($p = 0.037$). The diagnostic value of CNR in patients with the IVC type was higher

Zhengzhou University and the oral and maxillofacial surgery academic workstation of Zhengzhou (152PYSZ040).

Competing interests: The authors have declared that no competing interests exist.

than that in patients with mixed and HV type, while the diagnostic value of CNR was found to be the lowest for the HV type ($p = 0.043$).

Conclusion

A monochromatic energy level of 60 keV with 50% ASIR can significantly improve image quality in cases of BCS.

Introduction

Budd-Chiari syndrome (BCS) is characterized by obstruction in the hepatic venous outflow at the hepatic vein (HV) and the inferior vena cava (IVC). This results in the liver to heart reflux being affected thereby leading to a series of liver hemodynamic changes that manifest as a series of clinical symptoms[1]. Following the development of spectral computed tomography (CT), multi-parameter imaging has yielded abundant clinical diagnostic information. [2,3,4,5]. Currently, the application of spectral CT single-energy HV angiography predominantly pertains to portal vein(PV) angiography in patients with liver cirrhosis[6]. The present study of BCS CT angiography was limited to investigating the image quality of the best contrast-to-noise ratio (CNR) in single energy imaging for the PV, HV, and the IVC [7]. The primary aim of the study was to evaluate the quality of BCS angiography images of the spectral CT via single energy imaging combined with adaptive statistical iterative reconstruction(ASIR), and compare the image quality of different BCS types, in an effort to improve the quality of BCS angiography.

Materials and methods

Patients

The total of 62 BCS patients included in the study (41 men and 21 women, mean age 45.17 ± 11.13 years, age range 18–74 years) were diagnosed via surgery or Digital Subtraction Angiography(DSA) between May 2015 and September 2016. With regard to type distribution in the 62 cases, 11 were HV type, 7 were IVC type, and 44 were mixed (HV/IVC) type. The present study was approved by the Ethics Committee of The First Affiliated Hospital of Zhengzhou University, and all patients provided informed written consent before examination.

CT examination

Unenhanced and two-phase contrast-enhanced CT examinations were performed using the Discovery CT 750 system (GE Healthcare, Wisconsin, USA) in a craniocaudal direction in spectral imaging mode, with an individual contrast agent, a dual flow rate of injection of contrast medium, and utilization of the portal vein trigger scan mode. After spectral CT, all patients underwent unenhanced imaging in a conventional helical mode at a tube voltage of 140kVp. Patients were then injected with non-ionic contrast medium (Iohexol Injection, Optiray 350, GE Healthcare through antecubital venous access at a rate of 2–4 mL/s (4 mL/s for total of 180% and then 2 mL/s for total of 20% and 2 mL/s for 40 mL saline) for a total of 80–140 mL (1.6 mL/kg) during the portal venous phase (PVP) and the hepatic venous phase (HVP). The imaging delay for PVP imaging was determined by automated image-triggering software (Smart Prep, GE Healthcare). PVP imaging was automatically begun 30 s after the trigger attenuation threshold (120 Hounsfield units) was reached at the level of the PV trunk

and its branches. HVP imaging began 45 s after PVP imaging. PVP and HVP acquisitions were performed in the spectral imaging mode with a single tube. Other imaging parameters were slice thickness—5 mm, slice interval 5 mm, automatic tube current, rotation speed (gantry rotation time) - 0.8 s and helical pitch—0.984:1.

Image analyses

The single energy images were derived from spectral CT (slice thickness 1.25 mm) combined with ASIR (from 0 to 100%). The reconstructed images were processed with GSI Volume Viewer software and an AW 4.6 workstation (GE HealthCare) to measure and record relevant parameters. Comprehensive post-processing technology is used to display vascular diseases clearly and intuitively. (Fig 1).

For images at each energy level with ASIR, the mean CT-derived values (in Hounsfield units) of vessels (*i.e.*, PV, HV, and IVC) were assessed by manually placing circular or ovoid ROIs, which were drawn at the centrally within the segment (mean pixel number 57, range 34–85) from three contiguous slices. Mean CT data for the hepatic parenchyma and pancreas were obtained by manually placing circular ROIs at the same slice (mean pixel number 280, range 210–375). In cases where they were present, areas of focal changes in parenchymal density and large vessels were carefully avoided. A global assessment of image noise, defined as the standard deviation of the pixel values from a circular or ovoid ROI (mean pixel number 120, range 70–170) drawn in a homogeneous region of the subcutaneous fat of the anterior abdominal wall, was performed. To ensure consistency, all measurements were repeated three times at the three contiguous imaging levels, and average values were calculated. For all measurements the size, shape, and position of the ROIs were kept consistent between the two phases by applying the copy-and-paste function.

The lesion-to-liver CNR was calculated via the following equation: $CNR = (CT_1 - CT_2) / SD_2$. CT_1 for the CT value of the blood vessel, hepatic parenchyma and pancreas, CT_2 for the CT value of the subcutaneous fat, SD_2 for the standard deviation of the subcutaneous fat.

Subjective evaluation standard for image quality

Readers recorded the number of lesions, lesion size (defined as the maximum diameter measured with an electronic ruler on transverse images), and segmental location according to the anatomical segmentation schemes of Couinaud and Bismuth on a standardized template. For

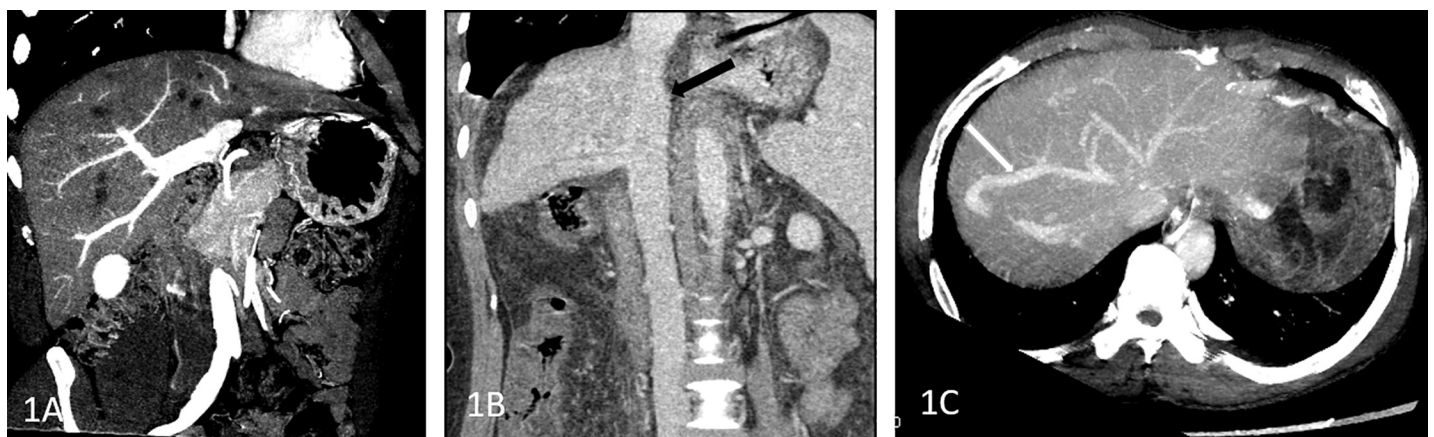


Fig 1. Vascular reconstruction of PV, HV, and IVC. A maximum intensity projection (MIP) image of the PV, showing the PV trunk and its branches clearly; Fig 1B curve planar reformation (CPR) image of the IVC, showing the IVC patency (black arrow); Fig 1C maximum intensity projection (MIP) image of the HV, showing the left HV, HV and right HV occlusion, subhepatic vein open, through the auxiliary hepatic vein (white arrow) into IVC.

<https://doi.org/10.1371/journal.pone.0204797.g001>

overall image quality [8], the scoring scale was as follows: 5 = no obvious image noise or artifacts, sharp anatomical structure and satisfactory detail; 4 = mild image noise and artifacts, less clear anatomical structure and detail; 3 = moderate image noise and artifacts, reduced confidence in details but anatomical structure still relatively clear; 2 = severe image noise and artifacts, confidence in details and anatomical structure reduced, diagnosis questionable; and 1 = severe image noise and artifacts, non-diagnostic.

With regard to BCS, a different subjective scoring system incorporating diagnostic confidence was evaluated. Scoring criteria are [9]: 1 = unclear, cannot be diagnosed; 2 = Half clear, diagnostic confidence < 50%; 3 = Clear, diagnostic confidence 50% to 90% - 3 points; 4 = Very clear, diagnostic confidence > 90%.

Statistical analysis

The SPSS 21.0 software package (IBM Corporation, Armonk, NY, USA) was used for statistical analysis. Normality of distribution variance homogeneity tests were applied to the data. The choice of ASIR weight value at a 60 keV monochromatic energy level and the variation in image quality of different BSC types were analyzed via one-way ANOVA. The Kruskal-Wallis H test was used to assess the overall image quality scores of the three groups of images. $p < 0.05$ was deemed to indicate statistical significance.

Results and discussion

Comparison of CNRs in the PV trunk, HV, IVC, hepatic parenchyma and pancreas at different ASIR weight values

CNR tended to increase with the increase in ASIR weight in the range of 0–100% ASIR weight at a 60 keV monochromatic energy level. CNR values were lowest at 0% ASIR, and highest at 100% ASIR. The difference in the PV trunk, HV, IVC, hepatic parenchyma, and pancreas CNRs from 0% to 100% ASIR weight was statistically significant ($p < 0.05$) (Fig 2).

Subjective scoring of different ASIR weight values

The image quality of the ASIR weight value from 0% to 50% increases, and 50% to 100% decreases, the image quality does not improve with the increasing ASIR weight value. The highest overall image score is at 50%. (Fig 3)

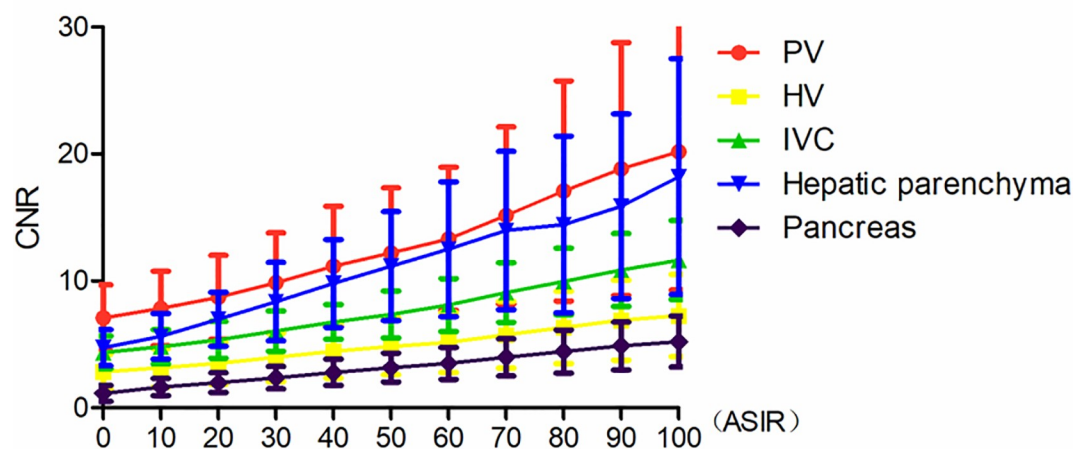


Fig 2. CNR values in the PV trunk, HV, IVC, hepatic parenchyma, and pancreas at 60keV. As the weight value of ASIR increased, the CNR value gradually increased.

<https://doi.org/10.1371/journal.pone.0204797.g002>

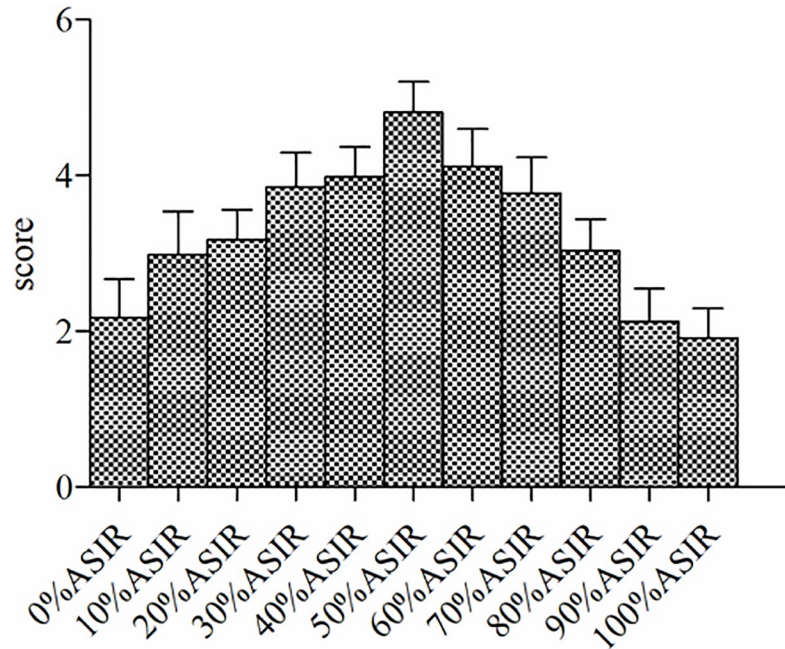


Fig 3. Overall image quality subjective with ASIR weight value curve. Fig 3 shows that the image quality of the ASIR weight value from 0% to 50% increases, and 50% to 100% decreases.

<https://doi.org/10.1371/journal.pone.0204797.g003>

Comparison of CNR values in different BCS types

CNR values of the PV trunk, HV, hepatic parenchyma and pancreas in the IVC type were significantly higher than those in the mixed type and HV type, and with the exception of the PV trunk, these were statistically significant. The CNR of the IVC in the HV type was greater than that of the mixed type and the IVC type and the difference was statistically significant ($p < 0.05$). The CNR of the IVC in the mixed type was lower than that of the HV type ($p = 0.028$, $p < 0.05$). The CNR of the HV and hepatic parenchyma in the mixed type was lower than that in the IVC type ($p = 0.016$ and 0.038 , $p < 0.05$), and the CNR of pancreas in the IVC type was higher than that in the HV type, ($p = 0.037$, $p < 0.05$). (Table 1, Fig 4)

Diagnostic confidence subjective score for different types of BCS

Diagnostic confidence was highest for the IVC type and lowest for the HV type. The difference was statistically significant ($p = 0.043$), (Table 2).

Table 1. Comparison of CNR values for the PV trunk, HV, IVC, hepatic parenchyma and pancreas in different BCS types (mean ± SD).

Type	Cases	PV trunk	HV	IVC	Hepatic parenchyma	Pancreas
Mixed	44	13.74±3.76	4.40±1.51	3.64±1.59	5.83±1.49	2.09±1.05
HV	11	12.35±3.15	4.13±1.22	5.01±1.18	5.70±1.21	1.57±0.58
IVC	7	14.73±3.13	6.26±1.63	3.72±1.29	7.42±1.90	2.82±1.13
F Value		1.042	4.230	3.655	3.542	3.351
P Value		0.359	0.019	0.032	0.035	0.042

CNR, contrast-to-noise ratio; PV, portal vein; HV, hepatic vein; IVC, inferior vena cava; BCS, Budd-Chiari syndrome; SD, standard deviation. $p < 0.05$ was considered statistically significant.

<https://doi.org/10.1371/journal.pone.0204797.t001>

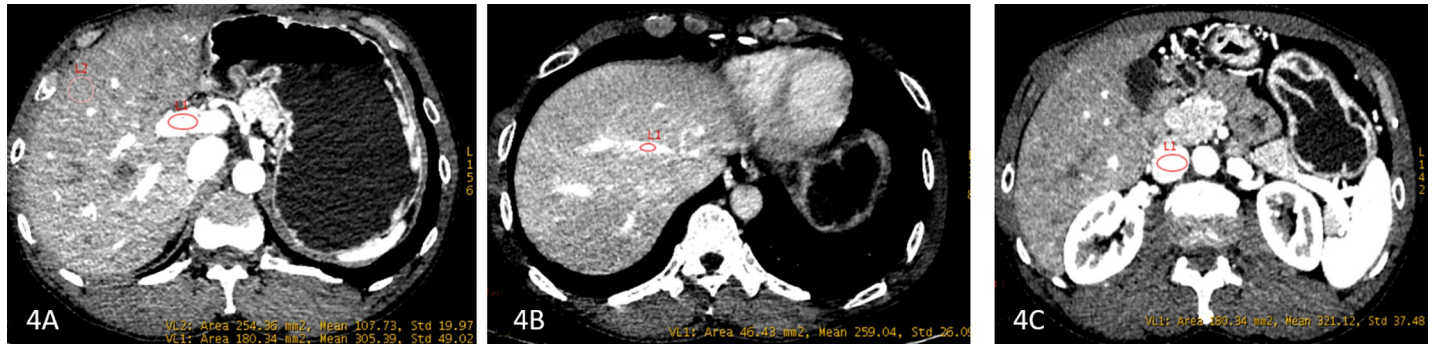


Fig 4. The CNR values of PV trunk, HV, IVC and hepatic parenchyma. Female, 57 years old, imaging diagnosis of BCS (HV type). Fig 4A–4C, Axial images, showed PV trunk, HV and IVC. The CNR values of PV trunk, HV, IVC and hepatic parenchyma were: 12.02, 4.09, 4.89, 5.64 and 1.61 respectively.

<https://doi.org/10.1371/journal.pone.0204797.g004>

Spectral CT scanning can simultaneously yield mixed energy and monochromatic-energy images (40–140 keV) [10,11,12,13]. In general, the low energy levels with high contrast and high noise. Reconstruction algorithms are one the important factors that affect image quality. ASIR is an iterative reconstruction algorithm of the data based on the noise reduction model. A reduction in the radiation dose also helps reduce the noise as has been previously demonstrated [13,14,15]. The adaptive method is based on a complete understanding of the noise properties and correcting suppressing them to get achieve clearer image.

Theoretically, the higher the ASIR weight value, the stronger the noise reduction capability. However, if the ASIR weight value increases beyond a certain point (say, approximately 80% ASIR), then the contrast in the image decreases significantly [16]. When the ASIR increases to more than 60%, the spatial resolution begins to decline as reported by Singh *et al* [17]. Therefore in order to maintain the spatial resolution of the image in an abdominal scan, the ASIR weight value should not exceed 60%. Studies have shown that the quality of chest and abdomen scan images decreases with increases in an ASIR weight value and so it is best to maintain ASIR weight value between 40%-60% [5,18].

In the current study, the ASIR weight value of the single energy image at a 60 keV monochromatic energy level was set from 0% to 100%, and the noise reduction rate of the image gradually increased with increasing ASIR weight value. At 0% ASIR the image noise reduction rate was the lowest, and at 100% it was the highest. CNR values gradually increased with increasing ASIR weight. CNR values were found to gradually increase with the increase in ASIR weight values. Subjective scoring results showed a decrease in score as ASIR increased beyond a point. When image noise was large, the score was low with ASIR weight value ranging from 0% to 20%. The spatial resolution began to reduce with ASIR weight value ranging from 70% -100%, and the image quality as well as the score was low with a "fuzzy" effect

Table 2. Diagnostic confidence subjective score for different types of BCS.

Group	Score of 1	Score of 2	Score of 3	Score of 4	Total	χ^2	<i>p</i> Value
Mixed type	0	9	23	12	44	6.310	0.043
HV type	0	4	7	0	11		
IVC type	0	0	4	3	7		

p < 0.05 on behalf of the difference was statistically significant.

<https://doi.org/10.1371/journal.pone.0204797.t002>

apparent in the image. Image quality acceptable at 30%-60% ASIR. The overall image score was the highest at 50% weight value. With higher ASIR value reconstruction, the spatial resolution of the image gets reduced and the noise value of the image changes leading to image distortion that cannot meet diagnostic requirements.

BCS types differ with regard to pathophysiological basis, clinical manifestation, clinical treatment, and prognosis [19,20]. Based on whether there were HV or IVC pathological changes, BCS was divided into HV type, IVC type and mixed type in the current study. The CNR values (except IVC) of the IVC type were greater than those of the HV type and mixed types. This is because the lesions simply involve the IVC and the obstruction of blood flow in the IVC, the reduction of blood flow rate and even reverse, which leads to lower inferior vena cava enhancement with relatively lower CNR. The CNR value of the IVC in the HV type was significantly greater than those of the mixed type and the HV type. This may be related to the simple involvement of hepatic veins, and IVC patency, which may result in the effect of IVC vascular enhancement being less. When we assess the diagnostic value of CT images, the diagnostic confidence of patients with the IVC type is higher than that of patients with the mixed type and the HV type, and the diagnostic confidence patients with the HV type is the lowest. This may be because the HV is thin, or the scanning phase is not accurate thus leading to unclear HV display. Additionally, due to HV occlusion and the formation of intrahepatic collateral vessels, blood vessels may appear unclear.

Conclusion

In conclusion, spectral CT provides a set of monochromatic energy levels that improved image quality in cases of BCS when combined with ASIR reconstruction technology. A monochromatic energy level of 60 keV in conjunction with 50% ASIR may be the best combination for reducing noise while providing higher overall image quality.

Acknowledgments

The present manuscript was supported by the National Natural Science Foundation of China (grant no. 81402231), the Basic and Frontier Technology Research Projects by Science and Technology Department of Henan (grant no. 142300410315).

Author Contributions

Conceptualization: Lei Su, Liyang Chang.

Data curation: Lei Su, Qiang Sun, Yan Wu.

Funding acquisition: Qiang Sun.

Investigation: Yan Wu.

Project administration: Jianbo Gao.

Resources: Lei Su, Liyang Chang.

Software: Lili Hu.

Supervision: Lili Hu.

Writing – original draft: Lei Su.

Writing – review & editing: Lei Su, Jianbo Gao.

References

1. Zhou PL, Yan L, Wu G, Han XW, Zhang WG (2017) Value of blood flow velocity on color Doppler ultrasonography for optimization of delay in scanning time on computed tomography venography in patients with Budd-Chiari syndrome and inferior vena cava obstruction. *Radiol Med*.
2. Liu L, Zhi X, Liu B, Zhang Y (2016) Utilizing gemstone spectral CT imaging to evaluate the therapeutic efficacy of radiofrequency ablation in lung cancer. *Radiol Med* 121: 261–267. <https://doi.org/10.1007/s11547-015-0602-5> PMID: 26612323
3. Yin XP, Zuo ZW, Xu YJ, Wang JN, Liu HJ, Liang GL, et al. (2017) The optimal monochromatic spectral computed tomographic imaging plus adaptive statistical iterative reconstruction algorithm can improve the superior mesenteric vessel image quality. *Eur J Radiol* 89: 47–53. <https://doi.org/10.1016/j.ejrad.2017.01.022> PMID: 28267548
4. Zhou Y, Xu H, Hou P, Dong JQ, Wang MY, Gao JB. (2016) Monochromatic Spectral Computed Tomography with Low Iodine Concentration Contrast Medium in a Rabbit VX2 Liver Model: Investigation of Image Quality and Detection Rate. *Acad Radiol* 23: 486–495. <https://doi.org/10.1016/j.acra.2015.12.001> PMID: 26795435
5. Li M, Zheng X, Gao F, Xiao L, Hua Y (2016) Spectral CT imaging of intranodular hemorrhage in cases with challenging benign thyroid nodules. *Radiol Med* 121: 279–290. <https://doi.org/10.1007/s11547-015-0601-6> PMID: 26612322
6. Zhao LQ, He W, Li JY, Chen JH, Wang KY, Tan L. (2012) Improving image quality in portal venography with spectral CT imaging. *Eur J Radiol* 81: 1677–1681. <https://doi.org/10.1016/j.ejrad.2011.02.063> PMID: 21444170
7. Su L, Dong J, Sun Q, Liu J, Lv P, Hu L, et al. (2014) Spectral CT imaging in patients with Budd-Chiari syndrome: investigation of image quality. *Cell Biochem Biophys* 70: 1043–1049. <https://doi.org/10.1007/s12013-014-0021-6> PMID: 24833430
8. Guimaraes LS, Fletcher JG, Harmsen WS, Yu L, Siddiki H, Melton Z, et al. (2010) Appropriate patient selection at abdominal dual-energy CT using 80 kV: relationship between patient size, image noise, and image quality. *Radiology* 257: 732–742. <https://doi.org/10.1148/radiol.10092016> PMID: 20959540
9. Kukuk GM, Gieseke J, Weber S, Hadizadeh DR, Nelles M, Träber F, et al. (2011) Focal liver lesions at 3.0 T: lesion detectability and image quality with T2-weighted imaging by using conventional and dual-source parallel radiofrequency transmission. *Radiology* 259: 421–428. <https://doi.org/10.1148/radiol.11101429> PMID: 21330565
10. Li H, He D, Lao Q, Chen X, Liu M, Yin B, et al. (2015) Clinical value of spectral CT in diagnosis of negative gallstones and common bile duct stones. *Abdom Imaging* 40: 1587–1594. <https://doi.org/10.1007/s00261-015-0387-y> PMID: 25725795
11. Chen S, Tan HY, Wu ZH, Sun CP, He JX, Li XC, et al. (2014) Imaging of olfactory bulb and gray matter volumes in brain areas associated with olfactory function in patients with Parkinson's disease and multiple system atrophy. *Eur J Radiol* 83: 564–570. <https://doi.org/10.1016/j.ejrad.2013.11.024> PMID: 24360232
12. Fang J, Zhang D, Wilcox C, Heidinger B, Raptopoulos V, Brook A, Brook A, et al. (2017) Metal implants on CT: comparison of iterative reconstruction algorithms for reduction of metal artifacts with single energy and spectral CT scanning in a phantom model. *Abdom Radiol (NY)* 42: 742–748.
13. Xiao H, Liu Y, Tan H, Liang P, Wang B, Su L, et al. (2015) A pilot study using low-dose Spectral CT and ASIR (Adaptive Statistical Iterative Reconstruction) algorithm to diagnose solitary pulmonary nodules. *BMC Med Imaging* 15: 54. <https://doi.org/10.1186/s12880-015-0096-6> PMID: 26576676
14. Vardhanabhuti V, Loader RJ, Mitchell GR, Riordan RD, Roobottom CA (2013) Image quality assessment of standard- and low-dose chest CT using filtered back projection, adaptive statistical iterative reconstruction, and novel model-based iterative reconstruction algorithms. *AJR Am J Roentgenol* 200: 545–552. <https://doi.org/10.2214/AJR.12.9424> PMID: 23436843
15. Lee SH, Kim MJ, Yoon CS, Lee MJ (2012) Radiation dose reduction with the adaptive statistical iterative reconstruction (ASIR) technique for chest CT in children: an intra-individual comparison. *Eur J Radiol* 81: e938–943. <https://doi.org/10.1016/j.ejrad.2012.06.013> PMID: 22795526
16. Okamoto EE, Sherbuk JE, Clark EH, Marks MA, Gandarilla O, Galdos-Cardenas G, et al. (2014) Biomarkers in *Trypanosoma cruzi*-infected and uninfected individuals with varying severity of cardiomyopathy in Santa Cruz, Bolivia. *PLoS Negl Trop Dis* 8: e3227. <https://doi.org/10.1371/journal.pntd.0003227> PMID: 25275382
17. Singh S, Kalra MK, Gilman MD, Hsieh J, Pien HH, Digumarthy SR, et al. (2011) Adaptive statistical iterative reconstruction technique for radiation dose reduction in chest CT: a pilot study. *Radiology* 259: 565–573. <https://doi.org/10.1148/radiol.11101450> PMID: 21386048

18. de Margerie-Mellon C, de Bazelaire C, Montlahuc C, Lambert J, Martineau A, Coulon P, et al. (2016) Reducing Radiation Dose at Chest CT: Comparison Among Model-based Type Iterative Reconstruction, Hybrid Iterative Reconstruction, and Filtered Back Projection. *Acad Radiol* 23: 1246–1254. <https://doi.org/10.1016/j.acra.2016.05.019> PMID: 27346234
19. Wang R, Meng Q, Qu L, Wu X, Sun N, Jin X. (2013) Treatment of Budd-Chiari syndrome with inferior vena cava thrombosis. *Exp Ther Med* 5: 1254–1258. <https://doi.org/10.3892/etm.2013.961> PMID: 23596497
20. Zhang F, Wang C, Li Y (2015) The outcomes of interventional treatment for Budd-Chiari syndrome: systematic review and meta-analysis. *Abdom Imaging* 40: 601–608. <https://doi.org/10.1007/s00261-014-0240-8> PMID: 25248791